AGU PUBLICATIONS

Geophysical Research Letters

RESEARCH LETTER
10.1002/2014GL061398

Key Points:
- A surf zone heat budget closes on diurnal and longer time scales
- Surf zone heating (by viscous dissipation) due to wave energy flux is important
- Internal waves, rip currents, and undertow contribute to heat budget residual

Correspondence to:
G. Sinnett,
gsinnett@ucsd.edu

Citation:
Sinnett, G., and F. Feddersen (2014), The surf zone heat budget: The effect of wave heating, *Geophys. Res. Lett.*, *41*, 7217–7226, doi:10.1002/2014GL061398.

Received 31 JUL 2014
Accepted 2 OCT 2014
Accepted article online 7 OCT 2014
Published online 23 OCT 2014

The surf zone heat budget: The effect of wave heating

Gregory Sinnett[1] and Falk Feddersen[1]

[1] Scripps Institution of Oceanography, La Jolla, California, USA

Abstract Surf zone incident wave energy flux is dissipated by wave breaking which through viscosity generates heat. This effect is not present in shelf heat budgets and has not previously been considered. Pier-based observations of water temperature in 1–4 m depth, meteorology, and waves are used to test a surf zone heat budget, which closes on diurnal and longer time scales. Wave energy flux is the second most variable term with mean contribution one fourth of the mean short-wave radiation. The heat budget residual has semidiurnal and higher-frequency variability and net cooling. Cross-shore advective heat flux driven by internal wave events, rip currents, and undertow contribute to this residual variability and net cooling. In locations with large waves, steeper beaches, or less solar radiation, the ratio of wave energy flux to short-wave radiation may be >1.

1. Introduction

The nearshore (defined as ≤ 6 m water depth) region is ecologically and economically critical. Invertebrates, fish, and birds make their home in the nearshore. The region is a center of tourism and recreation, fueling economic activity. Nearshore waters are often impacted by poor water quality [*Dorfman and Rosselot*, 2009], creating health risks for bathers [e.g., *Haile et al.*, 1999], thereby affecting coastal economies. The surf zone is the near-beach region where depth-limited wave breaking occurs (with typical width $L_{sz} = O(100)$ m, and depth typically twice the significant wave height). The region just seaward of the surf zone is denoted here as the inner shelf. Thus, the nearshore includes both the surf zone and inner shelf.

Water temperature variations play a critical ecological role in the nearshore and are linked to variation in mussel and barnacle growth rates [*Phillips*, 2005], egg mass production rates of the coastal crab *Cancer setosus* [*Fischer and Thatje*, 2008], and barnacle recruitment rates [*Broitman et al.*, 2005]. Temperature is also a tracer for nutrient delivery to coastal waters [e.g., *Omand et al.*, 2012]. Pathogen ecology in swimming waters is affected by temperature, including *Staphylococcus* [*Goodwin et al.*, 2012], *Enterroccus* [*Halliday*, 2012], and *Campylobacter* [*Hokajarvi et al.*, 2013].

Previous nearshore temperature observations have typically been made using a vertical array to measure temporal variability and vertical structure [e.g., *Winant*, 1974; *Pineda*, 1991]. Observations from the Scripps Institution of Oceanography (SIO) pier (La Jolla) in the Southern California Bight (http://cordc.ucsd.edu/projects/Piers/SIO/TChain/) reveal substantial temperature variability in 6 m water depth at high frequency (<11 h), semidiurnal (11–14.5 h), diurnal (18–33 h), and subtidal (>33 h) time scales (as defined by *Lerczak et al.* [2003]). In water as shallow as 1.5 m, high-frequency nonlinear internal waves with 1°C variation were observed on the summertime Dutch coast [*van Haren et al.*, 2012]. However, the dominant processes governing surf zone temperature variability are not known, and a surf zone heat budget has never previously been studied.

Heat budgets on the Northern California outer shelf (60–130 m water depth) show cross-shelf advection exports heat off shelf year-round [*Lentz*, 1987; *Dever and Lentz*, 1994]. In shallower water (12–26 m) net cross-shore heat advection keeps shallow waters cooler than predicted by local surface heating [*Fewings and Lentz*, 2011]. This cross-shore heat advection is influenced at subtidal time scales by stratification, along-shelf winds [*Austin*, 1999], and cross-shore wave-driven mass transport [*Fewings and Lentz*, 2011]. In addition, significant shelf temperature variations can be driven at diurnal time scales by sea breeze-driven upwelling [e.g., *Woodson et al.*, 2007] or solar heating [e.g., *Davis et al.*, 2011], and also driven at semidiurnal and shorter time scales by internal waves [e.g., *Omand et al.*, 2011; *Walter et al.*, 2012].

In contrast to the shelf, an additional process is *unique* to the surf zone heat budget. Incident wave energy flux F_{wave}, due to surf zone wave breaking, leads to turbulent dissipation [e.g., *Feddersen*, 2012a, 2012b],

©2014. American Geophysical Union. All Rights Reserved.

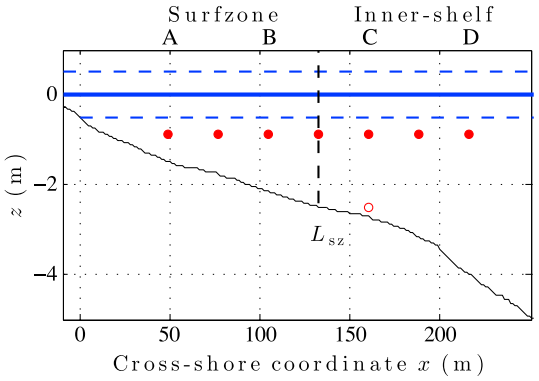

Figure 1. Cross-shore x distribution of thermistors mounted to the SIO pier (dots). A cross-shore bathymetry profile at the SIO pier is shown in black with mean sea level at $z = 0$ m (blue) and ± tide level (blue dashed). Seven thermistors (red) were deployed from 5 June to 23 July 2013. Specific cross-shore sensor locations are denoted A ($x = 49$ m), B ($x = 105$ m), C ($x = 160$ m), and D ($x = 216$ m). An additional thermistor was temporarily deployed from 5 June to 25 June at location C (open dot) 1.6 m below the near-surface thermistor. The outer surf zone boundary L_{sz} is set at $x = 132$ m (vertical black dashed line).

which by viscosity converts mechanical energy to heat. In addition, incident waves can also drive surf zone currents, which are largely frictionally balanced [e.g., *Feddersen et al.*, 1998], also generating heat. Incident F_{wave} is not fully converted into heat as there can be surf zone export of mechanical energy. However, as discussed in section 5, this is much smaller than the incident F_{wave}.

Observations from a cross-shore thermistor array mounted on the SIO pier (section 2) are used to test a simplified surf zone heat budget (section 3). The previously unconsidered wave energy flux term is significant, and the binned-mean heat budget closes to first order (section 4), although significant semidiurnal and higher-frequency variability in heat content is not resolved. The implications of wave energy flux heating of the surf zone and cross-shore advective heat flux are discussed in section 5. Results are summarized in section 6.

2. Experiment

A surf zone heat budget was tested with observations at the SIO pier for 47 days from 6 June to 23 July 2013. Six thermistors (Onset TidBit) were attached at $z = -0.9$ m below mean sea level to the north (shaded) portion of pier pilings at cross-shore (x) locations between $x = 49$ m and $x = 216$ m (where $x = 0$ m is at the mean low-tide shoreline) in mean water depths spanning $h = 1.5$ m to $h = 4$ m (Figure 1). The surf zone and inner-shelf bathymetry profile (Figure 1) was measured on day 46 of the experiment by a jet ski bathymetry surveying system. Four specific thermistor locations are denoted, from onshore to offshore, as A, B, C, and D. An additional deeper thermistor was deployed at C, 1.6 m below the upper thermistor and was active for 20 days. Offshore surface water temperature was recorded at the Scripps Coastal Data Information Program (CDIP) mooring site 201 (location E) 1.2 km from shore in approximately 39 m water depth. Data was removed during extreme low tides (vertical extents >0.69 m), when the thermistors might have been exposed to air (≈10% of all data).

Air temperature, humidity, winds, and tidal elevation were measured at the end of the SIO pier (near D). Incoming short-wave radiation also was measured on the SIO Pier with a LI-200SA Pyranometer sensor maintained by the SIO Climate Research Division. Hourly wave statistics, including significant wave height H_s, were provided by a virtual buoy (monitored and predicted points "MOP") at the SIO pier, from the real-time CDIP spectral refraction wave model, initialized from offshore buoys [*O'Reilly and Guza*, 1991, 1998]. This wave model has been used in studies of beach erosion [*Yates et al.*, 2009] and shoreline ground motions [*Young et al.*, 2013] in the Southern California Bight. During times when the pier-mounted SIO wave gauge was operational (May and late July to August 2013), the model demonstrates very high skill.

3. Surf Zone Heat Budget

The surf zone heat budget is written as a cross-shore and vertically integrated box model for heat content H, similar to a North Carolina inner-shelf heat budget in 13–26 m water depth [*Austin*, 1999]. With alongshore (y) uniform conditions, the surf zone heat content H (J m^{-1}) in a region from the shoreline $x = 0$ to the fixed surf zone width $x = L_{sz}$ is,

$$H = \rho c_p \int_0^{L_{sz}} \int_{-h(x)}^{0} T(x,z)\, dz\, dx, \quad (1)$$

©2014. American Geophysical Union. All Rights Reserved.

where ρ is the density, c_p is the specific heat capacity, and h is the water depth. The upper limit ($z = 0$ m) of the vertical integral is the mean sea surface. Heat content time variation is driven by the total heat fluxes F_{tot} into and out of the box, i.e.,

$$\frac{dH}{dt} = F_{tot}. \tag{2}$$

The total surf zone heat flux F_{tot} is,

$$F_{tot} = (Q_{sw} + Q_{lw} + Q_{lat} + Q_{sen})L_{sz} + F_{wave} + F_{adv}, \tag{3}$$

where the Q (W m^{-2}) terms are surface vertical heat fluxes, consisting of the water-entering short-wave (Q_{sw}) radiation, net long-wave (Q_{lw}) radiation, and latent (Q_{lat}) and sensible (Q_{sen}) heat fluxes. As written in (3), the Q terms are assumed cross-shore uniform but may differ between the surf zone, where waves are breaking, and farther offshore (but within the nearshore).

The F terms in (3) are cross-shore heat fluxes (W m^{-1}) evaluated at the surf zone boundary $x = L_{sz}$. The surf zone-specific cross-shore heat flux contribution from breaking surface gravity waves, F_{wave} (W m^{-1}), as in (4) is considered here for the first time. For narrowbanded waves, the cross-shore wave energy flux at the surf zone boundary is

$$F_{wave} = \frac{1}{16}\rho g H_s^2 c_g \cos(\theta), \tag{4}$$

where g is gravity, c_g is the group velocity at the peak frequency, and θ is the peak direction. Surf zone cross-shore advective heat flux F_{adv}, due to processes in the surf zone (such as undertow and rip currents) or shelf (internal waves), were not estimated here, and are discussed in section 5. Furthermore, the export of mechanical energy from the surf zone to inner shelf is shown to be small (section 5).

The resulting net surf zone heat flux, F_{net}, considered in this heat budget is

$$F_{net} = (Q_{sw} + Q_{lw} + Q_{lat} + Q_{sen})L_{sz} + F_{wave}, \tag{5}$$

which, as in (2), is balanced against dH/dt, i.e.,

$$dH/dt = F_{net}. \tag{6}$$

This heat budget (6) assumes that the gradient of cross-shore integrated alongshore (y) advective heat flux (i.e., terms related to $V dT/dy$, where V is the alongshore current) is negligible. On beaches with alongshore uniform bathymetry and incident wave field, time-averaged (hourly) alongshore mass, momentum, and turbulent kinetic energy flux gradients are weak [e.g., *Feddersen et al.*, 1998; *Feddersen and Guza*, 2003; *Feddersen*, 2012a]. Thus, alongshore heat flux gradients are expected to be weak as well.

The surf zone heat content H (1) was estimated with data from four surf zone thermistors and cross-shore integrating using the trapezoidal rule. Due to strong breaking wave-induced turbulence [e.g., *Feddersen*, 2012b], the surf zone is assumed to have vertically uniform temperature (i.e., well mixed), consistent with vertically uniform surf zone dye [*Hally-Rosendahl et al.*, 2014] and turbulent kinetic energy [*Ruessink*, 2010] observations. The outer limit of the surf zone was fixed at $L_{sz} = 132$ m (between B and C, vertical dashed line in Figure 1) which contained the surf zone at all times. However, at high tides and with small waves, wave breaking occurred farther onshore of $L_{sz} = 132$ m. The constant vertical integral upper limit ($z = 0$ m) fixes the mass of the surf zone. Thus, heat content changes (and associated fluxes) due to tidal-induced surf zone mass changes are not included here. The change in surf zone heat content, dH/dt, was estimated with centered differences.

Short-wave radiation above the water surface (Q_{sw}^{+}) was measured with a pier-end radiometer 10 m above the water surface. Water entering short-wave radiation Q_{sw} is estimated as $Q_{sw} = Q_{sw}^{+}(1-\alpha)$, where α is a solar zenith angle-dependent open ocean albedo (≈6%) parameterization [*Payne*, 1972]. As the surf zone is generally turbid with large optical attenuation, all water-entering Q_{sw} is assumed absorbed in the water column. Since the albedo of wet sand is small (≈6% [*Zhang et al.*, 2014]), any Q_{sw} reaching the bed will be absorbed by a thin sand layer, which will rapidly equilibrate with the turbulent water of the surf zone. Total (outgoing and incoming) long-wave radiation Q_{lw} is estimated with a standard bulk parameterization method using

©2014. American Geophysical Union. All Rights Reserved.

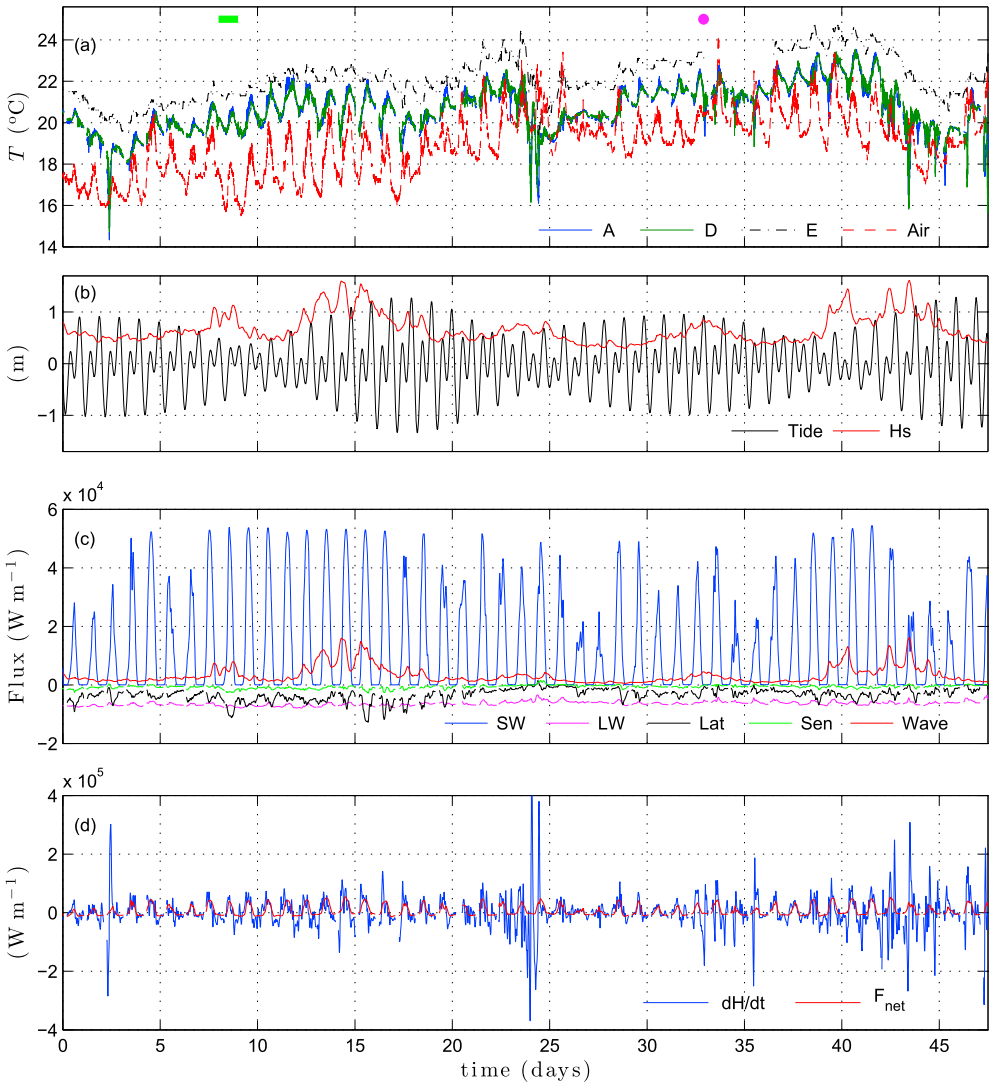

Figure 2. Time series of (a) water temperature at locations A (x = 49 m), D (x = 216 m), and E (CDIP buoy, x = 1200 m), and air temperature at SIO Pier (see legend). Note temperature at E is offset by 1.5°C for visibility. (b) Pier tidal elevation (black) and significant wave height H_s in 10 m depth (red). (c) Surf zone energy flux terms including water-entering short-wave ($Q_{sw}L_{sz}$) and net long-wave ($Q_{lw}L_{sz}$) radiative fluxes, sensible ($Q_{sen}L_{sz}$) and latent $Q_{lat}L_{sz}$) air-sea fluxes, and wave energy flux F_{wave}. (d) Cross-shore integrated surf zone heat budget terms dH/dt and F_{net}. The magenta dot at day 32 in plot (a) indicates the time of a strong internal wave event observed at locations C, B and A highlighted in Figure 4. The green bar over days 8 and 9 in Figure 2a corresponds to the time highlighted in Figure 5.

cloud cover, vapor pressure, and air and water temperature [*Josey et al.*, 1997]. Vapor pressure was calculated from sea surface temperature using the Antoine equation [*Thomson*, 1946]. Air-sea sensible (Q_{sen}) and latent (Q_{lat}) heat fluxes are estimated via the Coupled Ocean-Atmosphere Response Experiment (COARE) 2.5 bulk parameterization [*Fairall et al.*, 1996] using wind speed, air and water temperature, and humidity. All heat budget terms were low-pass filtered with a 2 h cutoff. Through controlled thermistor tests, the 2 h low-pass filtered dH/dt instrument noise level is estimated using (1) to be ≈ 300 W m^{-1}.

4. Results

Over the 47 day deployment, observed ocean temperature T spanned 14.5°C to 23.4°C (Figure 2a), with coherent variability at subtidal (>33 h) time scales. Diurnal variability was stronger closer to shore (A and D) than 1.2 km offshore at E. Air temperature was typically colder than the ocean, fluctuating subtidally and diurnally. Significant cross-shore T variation was also observed. The temperature difference between surf

©2014. American Geophysical Union. All Rights Reserved.

Table 1. Mean and Standard Deviation (SD) of Cross-Shore Integrated Surf Zone Heat Flux Terms (6) and (5): Short-Wave ($Q_{sw}L_{sz}$), Long-Wave ($Q_{lw}L_{sz}$), Latent ($Q_{lat}L_{sz}$), Sensible ($Q_{sen}L_{sz}$) Heat Fluxes, Wave Energy Flux (F_{wave}), Net Surf Zone Heat Flux F_{net}, and Surf Zone Heat Content Time Derivative dH/dt [a]

($\times 10^4$ W m^{-1})	$Q_{sw}\,L_{sz}$	$Q_{lw}\,L_{sz}$	$Q_{lat}L_{sz}$	$Q_{sen}L_{sz}$	F_{wave}	F_{net}	dH/dt	F_{res}
Mean	1.40	−0.63	−0.33	−0.06	0.33	0.70	0.18	−0.52
SD	1.69	0.07	0.20	0.05	0.29	1.73	5.52	5.10

[a] L_{sz} = 132 m.

zone location A and inner-shelf location D, ΔT_{AD} (separated by $\Delta x = 157$ m), varied significantly between −3°C and 2°C, generally at diurnal and shorter time scales (not shown). The deployment spanned several spring-tide (amplitude 1.3 m) and neap-tide (amplitude 0.3 m) cycles (Figure 2b, black), with the majority contribution from M2 and K1. The mean significant wave height, H_s, was 0.7 m (Figure 2b, red) but fluctuated on subtidal time scales with maximum and minimum of 1.6 m and 0.3 m, respectively.

The water-entering short-wave radiative heat flux ($Q_{sw}\,L_{sz}$) warms the surf zone, varies diurnally from zero at nighttime to peak daytime values $\approx 5 \times 10^4$ W m^{-1}, and is the largest surf zone heat budget term (blue curve in Figure 2c and Table 1). The net long-wave radiation ($Q_{lw}\,L_{sz}$) cools the surf zone and is largely steady at roughly half the time-averaged $Q_{sw}\,L_{sz}$ (magenta curve in Figure 2c and Table 1). The latent heat flux ($Q_{lat}\,L_{sz}$) and wave energy flux (F_{wave}) have similar magnitude and variability (black and red curves, respectively, in Figure 2c and Table 1), but cool and warm the surf zone, respectively. The wave energy flux term F_{wave} is on average one fourth of the short-wave radiative heating $Q_{sw}\,L_{sz}$ and is the second most variable term (Table 1), indicating it is an import factor in the surf zone heat budget. Estimated sensible heat flux ($Q_{sen}\,L_{sz}$) is small compared to other heat budget terms.

The net surf zone heat flux F_{net} (5) and surf zone heat content time derivative dH/dt are reasonably coherent at diurnal and longer time scales (Figure 2d), but dH/dt has more variability than F_{net} (Table 1) at semidiurnal and shorter time scales. This results in an unbinned heat balance (6) with low best fit skill (squared correlation $r^2 = 0.16$) and high heat budget residual $F_{res} = dH/dt - F_{net}$ (Table 1). A binned-mean heat balance, representative of diurnal and longer time scales, has a strong linear relationship between F_{net} and dH/dt with high best fit skill ($r^2 = 0.89$), near-one slope (± standard deviation) of 1.20(±0.06), and an intercept of -6×10^3 W m^{-1} (Figure 3). The slope and intercept of the binned-mean and unbinned heat balance are similar. The binned-mean heat balance high skill and the near-one slope indicates that, at diurnal and longer time scales, the heat budget closes to first order.

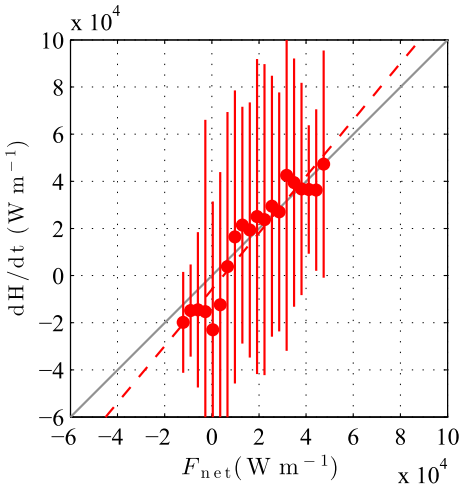

Figure 3. Surf zone heat budget (6): Binned-mean dH/dt versus F_{net} (solid red circles) and standard deviations (vertical red bars). The best fit line (red dashed) has a slope of 1.20 and an intercept of -6×10^3 W m^{-1}, with best fit skill of $r^2 = 0.89$.

The wave energy flux F_{wave}, the second most variable F_{net} term, plays a significant role in the surf zone heat budget. If F_{wave} is excluded from F_{net} (5), the binned-mean best fit slope is further from unity (1.33 ± 0.07) than if F_{wave} is included (1.20 ± 0.06). Thus, the wave energy flux helps balance the observed dH/dt variability, demonstrating its importance to the surf zone heat budget.

Over the 47 day experiment, the surf zone had net warming (positive $\langle dH/dt \rangle$ in Table 1, where $\langle\rangle$ represent a time average), but warmed slower (by ≈5200 W m^{-1}) than expected from $\langle F_{net} \rangle$, consistent with the heat budget's negative intercept (Figure 3). The surf zone net heat flux F_{net} variability is dominated (79% of variance) at diurnal (18–33 h) and subtidal (>33 h) time scales. The heat budget residual F_{res} variability far exceeds the 300 W m^{-1} expected noise level (Table 1)

©2014. American Geophysical Union. All Rights Reserved.

and is dominated (80% of variance) at semidiurnal (11–14.5 h) and higher-frequency (<11 h) time scales. Thus, processes (such as cross-shore heat advection) driving heat content net cooling and variability on semidiurnal and shorter time scales are missing from the estimated F_{net}. This is discussed further in section 5.

5. Discussion

At the La Jolla, CA, experiment site, the ratio of time-averaged (over the deployment) wave energy flux $\langle F_{wave} \rangle$ to time-averaged short-wave radiation $\langle Q_{sw} \rangle L_{sz}$ was ≈1/4, and the daily-averaged ratio $\langle F_{wave} \rangle / (\langle Q_{sw} \rangle L_{sz})$ varied between 0.05 and 1.1. This indicates that wave energy flux is important to the surf zone heat budget. The summer (June and July) deployment with long days and high solar zenith angle resulted in large daily-averaged short-wave radiation $\langle Q_{sw} \rangle = 106$ W m^{-2}. At this site, summer waves are generally small compared to winter. During different seasons or at other locations (such as the Oregon coast where there are strong waves and cloudy skies), the wave energy flux F_{wave} may be even more important in the surf zone heat budget. Assuming a planar beach slope β and normally incident shallow water waves ($c_g = \sqrt{gh}$) that break in depth h_b having constant $\gamma_b = H_s/h_b$ [e.g., *Thornton and Guza*, 1983], $L_{sz} = h_b/\beta$, and the ratio $F_{wave}/(Q_{sw}L_{sz})$, using (4), becomes

$$\frac{F_{wave}}{Q_{sw}L_{sz}} = \frac{\rho\beta\gamma_b^2(gh_b)^{\frac{3}{2}}}{16Q_{sw}}. \tag{7}$$

The ratio (7) gives the importance of wave energy flux relative to short-wave radiative solar heating and is proportional to beach slope β, γ_b^2, and $h_b^{3/2}$ (a function of H_s). For constant daily-averaged Q_{sw}, at steep beaches (where β is large and small surf zone width) or locations with large waves (where h_b is deeper), the importance of F_{wave} relative to $Q_{sw}L_{sz}$ in (3) increases. A Pacific Northwest winter case example with slope $\beta = 0.02$, $\gamma_b = 0.5$, and measured coastal November–March averaged short-wave radiation $\langle Q_{sw} \rangle = 52$ W m^{-2}, and large waves typical of this location ($H_s = 3$ m and $h_b = 6$ m) gives a average ratio (7) of 2.7. Thus, wave heating can be more important than daily-averaged short-wave radiative heating.

The incident F_{wave} may not be fully converted to heat in the surf zone, resulting in surf zone export of mechanical energy. One pathway is by shoreline wave reflection on nondissipative steep beaches. However, on dissipative beaches (such as this one), reflected wave energy flux was <0.03 of the incident F_{net} [e.g., *Elgar et al.*, 1994]. Rip currents or undertow could also export mechanical energy, which can be simply quantified as

$$h_b u^* \left(\frac{1}{2}\rho u^{*2}\right) \tag{8}$$

(units W m^{-1}), where u^* is an effective surf zone to inner-shelf exchange velocity that includes all potential exchange mechanisms. For a nearby beach with larger waves than typically observed here, $u^* \approx 10^{-2}$ m s^{-1} [*Hally-Rosendahl et al.*, 2014]. With $h_b \approx 2$ m (Figure 1), the surf zone export of kinetic energy (8) is approximately 10^{-3} W m^{-1}, 6 orders of magnitude less than the mean F_{net} of 3300 W m^{-1} (see Table 1). If instead $u^* = 10^{-1}$ m s^{-1} (a very large value), the surf zone export of kinetic energy becomes ≈1 W m^{-1}, still < 0.1% of the mean incident wave energy flux. Thus, the great majority of F_{net} must be dissipated within the surf zone.

The heat budget residual (Figures 2d and 3 and Table 1) has large semidiurnal and higher-frequency variability and a negative mean (residual cooling), analogous to the summertime shallow (12 m depth) shelf mean heat export by cross-shore advective processes [*Fewings and Lentz*, 2011]. Rip currents (e.g., seaward directed flow out of the surf zone [*Dalrymple et al.*, 2011]) can export heat from the surf zone [*Hally-Rosendahl et al.*, 2014], as likely can the undertow. The rip current- or undertow-induced F_{adv} can have contributions at a range of time scales from the mean, subtidal, tidal, and higher frequency. Internal waves can drive strong semidiurnal and higher-frequency nearshore temperature variability [e.g., *Winant*, 1974; *Pineda*, 1991]. This suggests that cross-shore advective heat flux F_{adv} due to these processes is important to the surf zone heat budget. Although F_{adv} was not measured here, the contribution from internal waves and surf zone processes (rip currents or undertow) to the surf zone heat content variability is examined qualitatively with two case examples.

©2014. American Geophysical Union. All Rights Reserved.

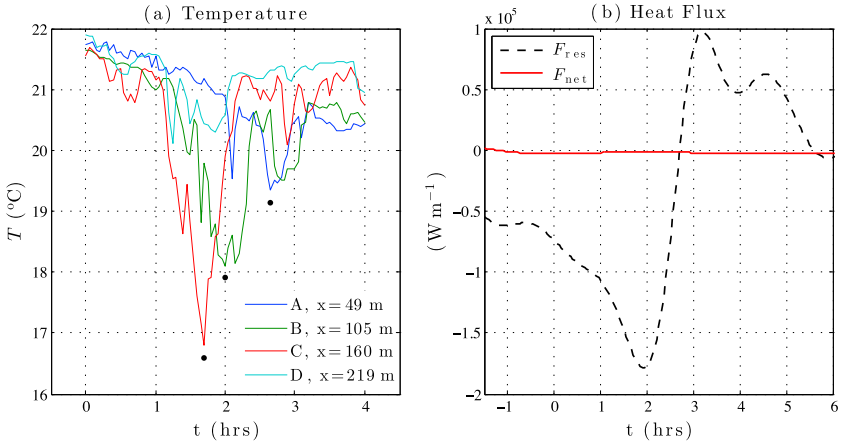

Figure 4. A 4 h cold event on 8 July (indicated by a magenta dot on day 32 in Figure 2a): (a) SIO water temperature T at locations A, B, C, and D versus time t ($t = 0$ h corresponds to 20:30 Pacific daylight time). Black dots at (A,B, and C) indicate the time of minimum temperature. (b) Net surf zone heat flux F_{net} (red) and the residual $F_{res} = dH/dt - F_{net}$ (black dashed) versus time t.

During the deployment, strong cold events were observed to propagate from the inner shelf (5 m depth) into the surf zone. A 4 h highly nonlinear internal wave (or bore) event demonstrates the internal wave contribution to high-frequency surf zone heat content variations (Figure 4). Internal waves have been observed seaward of the surf zone in $\geq$ 6 m water depth [e.g., *Winant*, 1974; *Pineda*, 1991, 1994; *Omand et al.*, 2011], and video observations of internal wave surface signatures just seaward of the surf zone suggest cross-shore propagation [*Suanda et al.*, 2014]. However, this is the first in situ observation of cross-shore internal bore propagation from $\approx$ 4 m depth through the surf zone.

During this event, $H_s \approx 0.82$ m and the ebbing spring tide varied $\approx$ 1 m. At $t = 1$ h, T_C ($x = 160$ m) dropped 4°C (from 21°C) in 0.6 h, subsequently rebounding to its initial level 0.5 h later (red curve in Figure 4a). The cold event arrived at B (55 m farther onshore) 0.3 h later, with an amplitude reduction to 3°C (green curve in Figure 4a). The cold event minimum arrived at A 0.6 h later with a reduced amplitude of $\approx$2°C (blue curve in Figure 4a). Within the surf zone (B and A), the cold event duration is longer than at the deeper C, and temperature does not recover to its pre-event level, indicating net cooling from this event. At location D (59 m offshore of C), no significant cold event is observed (cyan curve in Figure 4), indicating that the cold internal wave event only surfaced farther onshore. The inferred cold event propagation speeds ($C = \Delta x/\Delta t$) $C_{BC} = 0.05$ m s^{-1} and $C_{AB} = 0.03$ m s^{-1} are approximately consistent with a reduced-gravity shallow water phase speed appropriate for a gravity current.

During this cold event, the surf zone net heat flux F_{net} is very small (red curve in Figure 4b), yet the residual $dH/dt - F_{net}$ (black dashed curve in Figure 4b) is large with maximum magnitude of 1.7×10^5 W m^{-1}. This indicates that the internal wave-driven advective heat flux into or out of the surf zone is at times large, in part explaining the large high-frequency variability in dH/dt (Figure 2d). The area under the residual is negative (net cooling, black dashed curve Figure 4b) indicating that significant internal wave- or surf zone-driven mixing occurred.

Surf zone to inner-shelf heat exchange driven by surf zone processes is highlighted from a 2 day (14 and 15 June, days 9 and 10) ensemble-averaged neap-tide case. Between 09:00–14:30, the surf zone (A) and inner-shelf (D) warmed (Figure 5a) consistent with strong positive F_{net} (Figure 5b) dominated by solar heating. However, the surf zone (A) warmed more rapidly than the inner-shelf D (denoted differential warming, DW in Figure 5a), likely due to shallower surf zone depths, resulting in $\Delta T_{AD} \approx 0.4$°C after about 4 h. Subsequently, surf zone temperature equilibrated, while nearshore temperature continued to rise (14:30–18:00, EQ in Figure 5a). Both regions cool after 18:00. The surf zone temperature equilibration occurs even though the net heat flux F_{net} is positive (red curve in Figure 5b). Throughout EQ (14:30–18:00), the heat budget residual is negative (black dashed curve in Figure 5b), implying net surf zone cooling. The residual cooling time scale is much longer than that of the onshore propagating cold event (Figure 4). Furthermore, no large rapid temperature fluctuations (as in Figure 4) nor any sense of propagation were observed at the

©2014. American Geophysical Union. All Rights Reserved.

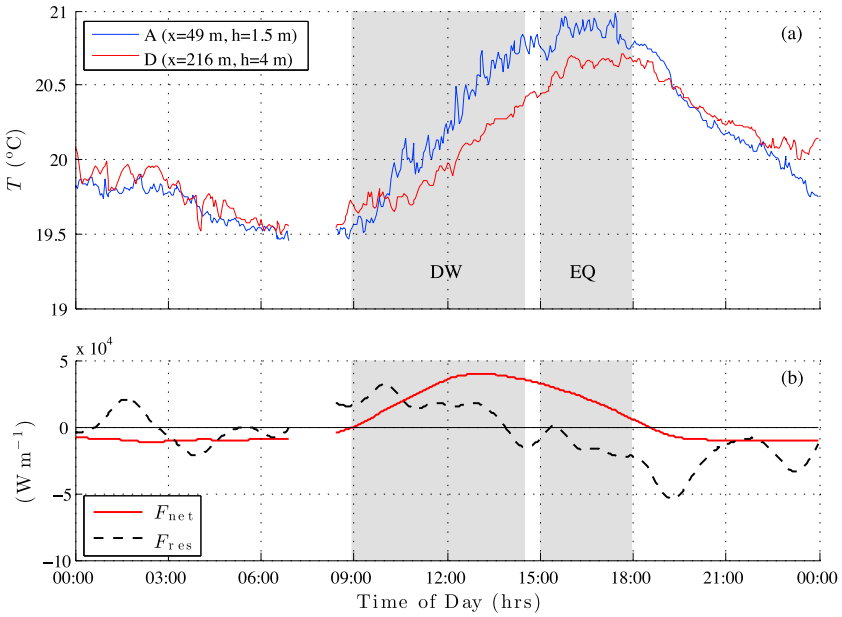

Figure 5. (a) Temperature at shallow surf zone location A (blue, $x = 49$ m, and $h = 1.5$ m) and the offshore, deeper location D (red, $x = 216$ m, $h = 4$ m) and (b) net surf zone heat flux F_{net} and the residual $F_{res} = dH/dt - F_{net}$ versus time of day. Temperature and solar radiation are ensemble averaged across 14 and 15 June (neap tide, days 8 and 9 highlighted by a green bar in Figure 2a). Periods of differential warming (DW, 9:00–14:30) and equilibration (EQ, 15:00–18:00) are highlighted.

thermistors. It is unlikely that a cold bore event was present below the surf zone thermistors (0.5–1.4 m above the bed, Figure 1), but not detected. Thus, the residual surf zone cooling during EQ is not due to internal waves. During EQ, the net residual cooling ($\approx 2.5 \times 10^4$ W m^{-1}) is also similar to the 2×10^4 W m^{-1} transient rip current-induced surf zone to inner-shelf heat flux inferred by *Hally-Rosendahl et al.* [2014]. Thus, this example of residual surf zone cooling is likely also due to surf zone to inner-shelf exchange induced by surf zone processes (undertow or rip currents). Larger waves drive larger rip currents [e.g., *Dalrymple et al.*, 2011]. Thus, feedback between wave energy flux and advective rip currents may also exist, such that as larger waves provide heat to the surf zone, some of that heat is advected offshore in more intense rip currents.

In addition to the large semidiurnal and high-frequency time scale heat budget residual, the binned-mean dH/dt variability is 20% larger than the binned-mean F_{net} variability (best fit slope is 1.2). Many factors may contribute to this, including estimating heat content (1) with only four thermistors, neglecting bathymetric $h(x)$ evolution, or assuming no stratification. In addition, the tidal sea surface variation, inducing surf zone mass and thereby heat content variations, is neglected. The vertical motion of the tides would lift and lower any surf zone stratification past the thermistors aliasing the dH/dt estimate. At the seaward of the surf zone location C (Figure 1), a second thermistor was deployed for the first 20 days 1.6 m below the upper thermistor. During this time, the root-mean-square stratification was 0.06°C m^{-1}. Using the observed tidal amplitudes, this results in a tidally induced apparent heat content variation of 2×10^3 W m^{-1}, small relative to F_{res} (Table 1). However, within the surf zone, strong breaking wave-induced mixing is expected to result in weaker stratification as with other tracers [e.g., *Hally-Rosendahl et al.*, 2014; *Ruessink*, 2010]. The near closure of the binned-mean heat budget justifies the neglect of the alongshore heat flux gradients. Wind-generated spray in the open ocean has been shown to strongly affect latent (Q_{lat}) and sensible (Q_{sen}) heat fluxes [*Andreas et al.*, 2008]. The COARE 2.5 parameterization for Q_{lat} and Q_{sen} used here does not include depth-limited breaking spray effects. Surf zone depth-limited wave breaking generates spray at least an order of magnitude larger than just offshore [*van Eijk et al.*, 2011]. Thus, surf zone latent and sensible heat fluxes may be under-represented, which could result in the best fit slope above one and net cooling. The heat flux between sediment and the surf zone (e.g., as on tidal flats [*Rinehimer and Thomson*, 2014; *Kim et al.*, 2010]) is neglected in (3) as here the beach slope and tidal amplitudes are 25× larger and 3× smaller, respectively, than on these tidal flats.

©2014. American Geophysical Union. All Rights Reserved.

6. Summary

An experiment was conducted at the Scripps Institution of Oceanography (SIO) pier from 6 June to 23 July 2013 to determine the importance of the onshore wave energy flux F_{wave} to the surf zone heat budget, which up to now had not been considered. Pier-deployed thermistors measured surf zone and inner-shelf water temperature, with concurrent pier-based meteorological measurements and model wave energy flux estimates. The surf zone heat budget balances the time variation of vertical and cross-shore (over the surf zone width L_{sz}) integrated heat content dH/dt with surf zone water-entering short-wave and net long-wave radiation, latent and sensible heat fluxes (Q_{sw} L_{sz}, Q_{lw} L_{sz}, $Q_{lat}L_{sz}$, and $Q_{sen}L_{sz}$, respectively) and the cross-shore wave energy flux F_{wave}. Short-wave radiation was the largest term in the surf zone heat budget. Time-averaged long-wave radiation, latent and sensible heat flux cooled the surf zone. The wave energy flux F_{wave} heated the surf zone, was on average ≈1/4 of the daily averaged short-wave radiative heating and was the second most variable term in the heat budget. The binned-mean heat budget, representative of diurnal and longer time scales, had high skill ($r^2 = 0.89$) and a slope near one, indicating the surf zone heat budget closed to first order.

The heat balance had unexplained residual variability at semidiurnal and high-frequency time scales, and residual net cooling (≈5200 W m^{-1}). Cross-shore (surf zone to inner-shelf) advective heat fluxes due to nonlinear internal waves (causing 3°C surf zone temperature variation in 0.6 h) and surf zone processes such as rip currents and undertow, (at times exporting $\approx 2.5 \times 10^4$ W m^{-1}) contributed to the high-frequency and net heat budget residual.

Excluding the wave energy flux F_{wave} from the binned-mean heat budget results in a best fit slope farther from one, further demonstrating the importance of breaking wave-induced heating to the surf zone heat budget. A scaling for the ratio of F_{wave} to short-wave surf zone heat flux ($Q_{sw}L_{sz}$) shows that at locations where there are large waves, a large beach slope, or less solar insolation, the ratio may be >1.

Acknowledgments

Support was provided by the National Science Foundation (NSF) and the Scripps GK12 program. Field data were collected with help from Kent Smith, Rob Grenzeback, Brian Woodward, Dennis Darnell, and Kai Hally-Rosendahl. Dan Cayan of the SIO Climate Research Division and Doug Alden and Spencer Kawamoto of the SIO Hydraulics Laboratory provided the short-wave radiative data which are available at http://meteora.ucsd.edu/weather/observations/sio_other/sites/stn_21.html. Pier end meteorological data were provided by the SIO Climate Research Division. The SIO Coastal Data Information Program (CDIP) provided wave measurements, and William O'Reilly and Corey Olfe provided wave model information for the SIO pier. Comments from two anonymous reviewers significantly improved this manuscript. Thank you.

Lisa Beal thanks Stephen Monismith and one anonymous reviewer for their assistance in evaluating this paper.

References

Andreas, E. L., P. O. G. Persson, and J. E. Hare (2008), A bulk turbulent air-sea flux algorithm for high-wind, spray conditions, *J. Phys. Oceanogr.*, *38*(7), 1581–1596, doi:10.1175/2007JPO3813.1.

Austin, J. A. (1999), The role of the alongshore wind stress in the heat budget of the North Carolina inner shelf, *J. Geophys. Res.*, *104*(C8), 18,187–18,203, doi:10.1029/1998JC900122.

Broitman, B., C. Blanchette, and S. Gaines (2005), Recruitment of intertidal invertebrates and oceanographic variability at Santa Cruz Island, California, *Limnol. Oceanogr.*, *50*(5), 1473–1479.

Dalrymple, R. A., J. H. MacMahan, A. J. H. M. Reniers, and V. Nelko (2011), Rip currents, *Annu. Rev. Fluid Mech.*, *43*, 551–581, doi:10.1146/annurev-fluid-122109-160733.

Davis, K. A., S. J. Lentz, J. Pineda, J. T. Farrar, V. R. Starczak, and J. H. Churchill (2011), Observations of the thermal environment on Red Sea platform reefs: A heat budget analysis, *Coral Reefs*, *30*, 25–36, doi:10.1007/s00338-011-0740-8.

Dever, E. P., and S. J. Lentz (1994), Heat and salt balances over the Northern California shelf in winter and spring, *J. Geophys. Res.*, *99*(C8), 16,001–16,017, doi:10.1029/94JC01228.

Dorfman, M., and K. S. Rosselot (2009), Testing the waters: A guide to water quality at vacation beaches, *Tech. Rep.*, National Resources Defense Council, New York. [Available at www.nrdc.org/water/oceans/ttw/ttw2009.pdf.]

Elgar, S., T. Herbers, and R. T. Guza (1994), Reflection of ocean surface gravity waves from a natural beach, *J. Phys. Oceanogr.*, *24*, 1503–1511.

Fairall, C., E. Bradley, D. Rogers, J. Edson, and G. Young (1996), Bulk parameterization of air-sea fluxes for tropical ocean-global atmosphere coupled-ocean atmosphere response experiment, *J. Geophys. Res.*, *101*(C2), 3747–3764.

Feddersen, F. (2012a), Observations of the surfzone turbulent dissipation rate, *J. Phys. Oceanogr.*, *42*, 386–399, doi:10.1175/JPO-D-11-082.1.

Feddersen, F. (2012b), Scaling surfzone turbulence, *Geophys. Res. Lett.*, *39*, L18613, doi:10.1029/2012GL052970.

Feddersen, F., and R. T. Guza (2003), Observations of nearshore circulation: Alongshore uniformity, *J. Geophys. Res.*, *108*(C1), 3006, doi:10.1029/2001JC001293.

Feddersen, F., R. T. Guza, S. Elgar, and T. H. C. Herbers (1998), Alongshore momentum balances in the nearshore, *J. Geophys. Res.*, *103*, 15,667–15,676.

Fewings, M. R., and S. J. Lentz (2011), Summertime cooling of the shallow continental shelf, *J. Geophys. Res.*, *116*, C07015, doi:10.1029/2010JC006744.

Fischer, S., and S. Thatje (2008), Temperature-induced oviposition in the brachyuran crab Cancer setosus along a latitudinal cline: Aquaria experiments and analysis of field-data, *J. Exp. Mar. Biol. Ecol.*, *357*(2), 157–164, doi:10.1016/j.jembe.2008.01.007.

Goodwin, K. D., M. McNay, Y. Cao, D. Ebentier, M. Madison, and J. F. Griffith (2012), A multi-beach study of Staphylococcus aureus, MRSA, and enterococci in seawater and beach sand, *Water Res.*, *46*, 4195–4207, doi:10.1016/j.watres.2012.04.001.

Haile, R. W., et al. (1999), The health effects of swimming in ocean water contaminated by storm drain runoff, *Epidemiology*, *10*, 355–363.

Halliday, E. E. A. (2012), Sands and environmental conditions impact the abundance and persistence of the fecal indicator bacteria enterococcus at recreational beaches, PhD thesis, Mass. Inst. of Tech., Cambridge, Mass.

Hally-Rosendahl, K., F. Feddersen, and R. T. Guza (2014), Cross-shore tracer exchange between the surfzone and the inner-shelf, *J. Geophys. Res. Oceans*, *119*, 4367–4388, doi:10.1002/2013JC009722.

©2014. American Geophysical Union. All Rights Reserved.

Hokajarvi, A.-M., T. Pitkanen, H. M. P. Siljanen, U.-M. Nakari, E. Torvinen, A. Siitonen, and I. T. Miettinen (2013), Occurrence of thermotolerant Campylobacter spp. and adenoviruses in Finnish bathing waters and purified sewage effluents, *J. Water Health*, *11*(1), 120–134, doi:10.2166/wh.2012.192.

Josey, S. A., D. Oakley, and R. W. Pascal (1997), On estimating the atmospheric longwave flux at the ocean surface from ship meteorological reports, *J. Geophys. Res.*, *102*(C13), 27,961–27,972.

Kim, T., Y. Cho, K. You, and K. Jung (2010), Effect of tidal flat on seawater temperature variation in the southwest coast of Korea, *J. Geophys. Res.*, *115*, C02007, doi:10.1029/2009JC005593.

Lentz, S. J. (1987), A heat budget for the northern California shelf during CODE 2, *J. Geophys. Res.*, *92*(C13), 14,491–14,509, doi:10.1029/JC092iC13p14491.

Lerczak, J. A., C. D. Winant, and M. C. Hendershott (2003), Observations of the semidiurnal internal tide on the southern California slope and shelf, *J. Geophys. Res.*, *108*(C3), 3068, doi:10.1029/2001JC001128.

Omand, M. M., J. J. Leichter, P. J. S. Franks, A. J. Lucas, R. T. Guza, and F. Feddersen (2011), Physical and biological processes underlying the sudden appearance of a red-tide surface patch in the nearshore, *Limnol. Oceanogr.*, *56*, 787–801.

Omand, M. M., F. Feddersen, P. J. S. Franks, and R. T. Guza (2012), Episodic vertical nutrient fluxes and nearshore phytoplankton blooms in southern California, *Limnol. Oceanogr.*, *57*, 1673–1688, doi:10.4319/lo.2012.57.6.1673.

O'Reilly, W., and R. Guza (1991), Comparison of spectral refraction and refraction-diffraction wave models, *J. Waterw. Port Coastal Ocean Eng.-ASCE*, *117*(3), 199–215, doi:10.1061/(ASCE)0733-950X(1991)117:3(199).

O'Reilly, W., and R. Guza (1998), Assimilating coastal wave observations in regional swell predictions. Part I: Inverse methods, *J. Phys. Oceanogr.*, *28*(4), 679–691, doi:10.1175/1520-0485(1998)028<0679:ACWOIR>2.0.CO;2.

Payne, R. E. (1972), Albedo of the sea surface, *J. Atmos. Sci.*, *29*, 959–970.

Phillips, N. (2005), Growth of filter-feeding benthic invertebrates from a region with variable upwelling intensity, *Mar. Ecol. Prog. Ser.*, *295*, 79–89, doi:10.3354/meps295079.

Pineda, J. (1991), Predictable upwelling and the shoreward transport of planktonic larvae by internal tidal bores, *Science*, *253*(5019), 548–551, doi:10.1126/science.253.5019.548.

Pineda, J. (1994), Internal tidal bores in the nearshore: Warm-water fronts, seaward gravity currents and the onshore transport of neustonic larvae, *J. Mar. Res.*, *52*(3), 427–458, doi:10.1357/0022240943077046.

Rinehimer, J., and J. T. Thomson (2014), Observations and modeling of heat fluxes on tidal flats, *J. Geophys. Res. Oceans*, *119*, 133–146, doi:10.1002/2013JC009225.

Ruessink, B. G. (2010), Observations of turbulence within a natural surf zone, *J. Phys. Oceanogr.*, *40*(12), 2696–2712, doi:10.1175/2010JPO4466.1.

Suanda, S. H., J. A. Barth, R. A. Holman, and J. Stanley (2014), Shore-based video observations of nonlinear internal waves across the inner shelf, *J. Atmos. Oceanic Technol.*, *31*(3), 714–728.

Thomson, G. W. (1946), The Antoine equation for vapor pressure data, *Chem. Rev.*, *38*(1), 1–39.

Thornton, E. B., and R. T. Guza (1983), Transformation of wave height distribution, *J. Geophys. Res.*, *88*(C10), 5925–5938.

van Eijk, A. M. J., J. T. Kusmierczyk-Michulec, M. J. Francius, G. Tedeschi, J. Piazzola, D. L. Merritt, and J. D. Fontana (2011), Sea-spray aerosol particles generated in the surf zone, *J. Geophys. Res.*, *116*, D19210, doi:10.1029/2011JD015602.

van Haren, H., L. Gostiaux, M. Laan, M. van Haren, E. van Haren, and L. J. A. Gerringa (2012), Internal wave turbulence near a Texel beach, *PLOS ONE*, *7*(3), e32535, doi:10.1371/journal.pone.0032535.

Walter, R. K., C. B. Woodson, R. S. Arthur, O. B. Fringer, and S. G. Monismith (2012), Nearshore internal bores and turbulent mixing in southern Monterey Bay, *J. Geophys. Res.*, *117*, C07017, doi:10.1029/2012JC008115.

Winant, C. (1974), Internal surges in coastal waters, *J. Geophys. Res.*, *79*(30), 4523–4526, doi:10.1029/JC079i030p04523.

Woodson, C., et al. (2007), Local diurnal upwelling driven by sea breezes in northern Monterey Bay, *Cont. Shelf Res.*, *27*(18), 2289–2302, doi:10.1016/j.csr.2007.05.014.

Yates, M. L., R. T. Guza, and W. C. O'Reilly (2009), Equilibrium shoreline response: Observations and modeling, *J. Geophys. Res.*, *114*, C09014, doi:10.1029/2009JC005359.

Young, A. P., R. T. Guza, M. E. Dickson, W. C. O'Reilly, and R. E. Flick (2013), Ground motions on rocky, cliffed, and sandy shorelines generated by ocean waves, *J. Geophys. Res. Oceans*, *118*, 6590–6602, doi:10.1002/2013JC008883.

Zhang, Y., X. Wang, R. Hu, Y. Pan, and H. Zhang (2014), Variation of albedo to soil moisture for sand dunes and biological soil crusts in arid desert ecosystems, *Environ. Earth Sci.*, *71*(3), 1281–1288.

©2014. American Geophysical Union. All Rights Reserved.